Solution Structure and Backbone Dynamics of the Functional Cytoplasmic Subdomain of Human Ephrin B2, a Cell-Surface Ligand with Bidirectional Signaling Properties†

Jianxing Song,*,‡ Wim Vranken,‡ Ping Xu,‡ Richard Gingras,‡ Ryan S. Noyce,‡ Zhenbao Yu,§ Shi-Hsiang Shen,§ and Feng Ni*,§

Biomolecular NMR Group and Mammalian Cells Genetics Group, Biotechnology Research Institute, National Research Council Canada, 6100 Royalmount Avenue, Montreal, Quebec, Canada H4P 2R2

Received March 14, 2002; Revised Manuscript Received June 12, 2002

ABSTRACT: The cytoplasmic domain of B ephrins plays a central role in bidirectional signal transduction processes controlling pattern formation and morphogenesis, such as axon guidance, cell migration, segmentation, and angiogensis. In particular, the extremely conserved last 33-residue cytoplasmic subdomain was shown to bind to both a PDZ domain for one signaling pathway [Lu et al. (2001) *Cell 105*, 69−79] and an SH2 domain from an alternative signaling network [Cowan and Henkemeyer (2001) *Nature 413*, 174−179]. To date, no structural information is available for the cytoplasmic domain of ephrin B proteins. We report here a detailed NMR study on the structural and dynamic properties of the cytoplasmic domain of human ephrin B2. Our results reveal the following: (1) the N-terminal region of the cytoplasmic domain from residues 253 to 300 lacks the ability for structure formation and is particularly prone to aggregation; and (2) the C-terminal functional subdomain from residues 301 to 333 assumes two distinctive structural elements with residues 301−322 adopting a well-packed hairpin structure followed by a flexible C-terminal tail. Furthermore, the backbone ^{15}N relaxation data demonstrate that the hairpin structure has significantly limited backbone motions, indicating a high conformational stability for the folded structure. Therefore, while the flexible C-terminal tail is suitable for binding to the PDZ domain, the folded hairpin may represent a latent structure requiring phosphorylation-induced conformational changes for high-affinity interactions with the SH2 domain.

Signal transduction through receptor tyrosine kinases plays an essential role in the development of multicellular organisms. Recently, the Eph receptor tyrosine kinases and their ephrin ligands have been implicated to function at the interface between pattern formation and morphogenesis (*1*, *2*), a critical step for neural development (*3*−*5*) and vascular morphogenesis (*6*−*8*). Eph−ephrin-mediated signaling is conserved among metazoans, and related receptors and ligands have been identified in *C. elegans*, *Drosophila*, *Xenopus*, and other vertebrates. In the Eph−ephrin signaling systems, the distinction between receptors and ligands is not absolute since accumulating genetic and biochemical evidence supports the scenario that ephrin ligands can also in some cases act as "receptors". In other words, the same Eph and ephrin proteins can either send or receive signals, depending on the developmental context of the "receptor" (*8*−*10*). So far, eight mammalian ephrins have been identified, which can be grouped into two structural and functional families. Five ligands (ephrin-A1 to ephrin-A5) belong to family A which are linked to the cell membrane by a glycosylphosphatidylinositol (GPI) moiety, while there are three ligands (ephrin B1 to ephrin B3) in family B. B ephrins and their Eph receptors transmit signals bidirectionally, thus mediating contact-dependent cell−cell interactions involved in the guidance and assembly of cells (*11*, *12*).

The B ephrin family proteins are anchored to the cell surface, having an extracellular domain, a transmembrane fragment, and a cytoplasmic domain. The cytoplasmic domains contain approximately 82 amino acids and are conserved among the ephrin B family (Figure 1). In particular, the last 33 amino acids are extremely conserved, showing a remarkable 90−100% identity within the 3 members, but with no detectable sequence homology with other proteins (*13*−*18*). The striking conservation of the cytoplasmic domains alone, especially the last 33 residues, strongly suggests a unique functional role for the C-termini of the B ephrin molecules. Indeed, functional studies have identified the cytoplasmic domain of ephrin B as involved in the bidirectional signaling (*6*, *19*−*21*). During the course of our NMR[1] study, peptides corresponding to the C-terminal

† This work was supported by the National Research Council of Canada (NRCC Publication No. 44851).

* Correspondence should be addressed to either of these authors. F.N.: email Feng.Ni@nrc.ca; phone (514)-496-6729; fax (514)-496-5143. J.S.: email Jianxing.Song@nrc.ca.

‡ Biomolecular NMR Group.

§ Mammalian Cells Genetics Group.

[1] Abbreviations: GST, glutatione *S*-transferase; HPLC, high-performance liquid chromatography; NMR, nuclear magnetic resonance; NOE, nuclear Overhauser enhancement; NOESY, NOE spectroscopy; TOCSY, total correlation spectroscopy; HSQC, heteronuclear single-quantum coherence spectroscopy; *T*1, longitudinal relaxation time; *T*2, transverse relaxation time; CPMG, Carr−Purcell−Meiboom−Gill.

10.1021/bi025815u CCC: $22.00 Published 2002 by the American Chemical Society
Published on Web 08/10/2002

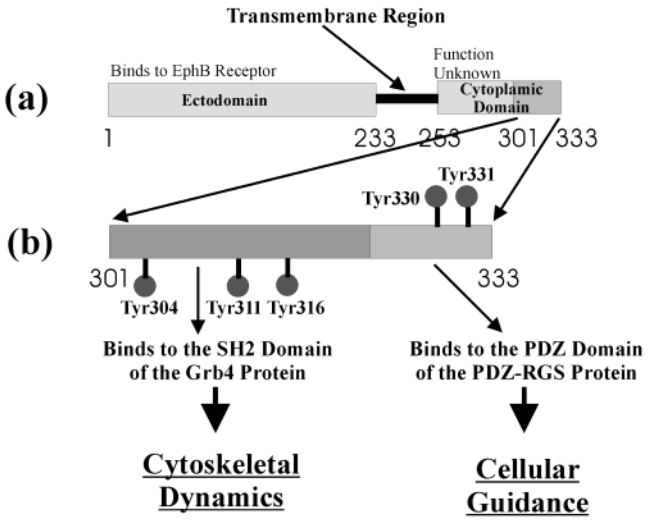

FIGURE 1: Schematic representation of the domain organization of human ephrin B2. (a) Entire human ephrin B2 protein is composed of an N-terminal extracellular domain (residues 1−233) that binds EphB receptors, a transmembrane region (residues 234−252), and the cytoplasmic domain (residues 253−333). Within the cytoplasmic domain, the functional role of residues 253−300 remains completely unknown, but residues 301−333 are highly conserved in the ephrin B family and are responsible for binding to all intracellular partners identified so far. (b) Expanded region of the cytoplasmic functional subdomain ephrin-$B2_{301-333}$ carrying all five functionally important tyrosine residues (Tyr304, Tyr311, Tyr316, Tyr330, and Tyr331). The phosphorylated N-terminal region of ephrin-$B2_{301-333}$ was identified to bind to the SH2 domain of the Grb4 protein, thereby mediating cytoskeletal dynamics (*21*), while the C-terminal part was found to interact with the PDZ domain of the PDZ−RGS protein, controlling the signaling for cellular guidance (*20*).

33 residues of ephrin B were also experimentally identified to bind to the PDZ domain of a novel PDZ−RGS protein (*20*) and to the SH2 domain of the Grb4 adaptor protein (*21*). At the same time, the bidirectional signaling mediated by interactions between B ephrins and the Eph receptor tyrosine kinases is only starting to be understood in structural terms. For example, the three-dimensional structures of the extracellular domain of ephrin B2 and its complex with Eph were reported recently (*9*, *22*). However, the structural properties of the cytoplasmic domain involved in the other half of the bidirectional signaling still remain completely unknown.

Our work reported here has focused on the structure characterization of the entire cytoplasmic domain and its dissected fragments by use of NMR spectroscopy. We found that the entire cytoplasmic domain or residues 253−333 and a subfragment encompassing residues 253−300 lack the ability to fold into uniquely defined three-dimensional structures and are especially prone to aggregation. Very unexpectedly, the functional subdomain over the last 33 residues, which contains all functionally important binding sites identified so far, is structured and adopts a well-packed hairpin followed by a flexible turn structure at the C-terminal region. Furthermore, in complete agreement with structure determination, backbone ^{15}N NMR relaxation data demonstrate that the two structural elements of the C-terminal functional subdomain have distinctive backbone motional properties. These results from our study provide valuable insights into the oligomerization property and functional interactions involving the cytoplasmic domain of B ephrins.

EXPERIMENTAL PROCEDURES

Cloning and Expression of the Cytoplasmic Domain and Its Subfragments. The DNA fragment encoding the cytoplasmic domain (residues 253−333) of human ephrin B2 (designated as ephrin-$B2_{253-333}$) was obtained by PCR on the vector pBTM116-SVC containing the human ephrin B2 gene. The PCR fragment was cloned into the expression vector pET-15b (Novagen) with *Nde*I/*Bam*HI restriction sites. The DNA sequence was confirmed by automated DNA sequencing. The recombinant His-tagged protein was expressed in BL21 and was subsequently purified by use of a Ni-agarose affinity column.

The DNA fragments encoding both ephrin-$B2_{253-300}$ and ephrin-$B2_{301-333}$ with amino acid sequences of $_{253}$RRRHRKHSPQ$_{262}$ HTTTLSLSTL$_{272}$ ATPKRSGNNN$_{282}$ GSEPSDIIIP$_{292}$ LRTADSVF$_{300}$ and $_{301}$CPHYEKVSGD$_{310}$ YGHPVYIVQE$_{320}$ MPPQSPANIY$_{330}$ YKV$_{333}$, respectively, were obtained by PCR and subsequently cloned into the pGEX-5X-1 expression vector as glutathione *S*-transferase fusion proteins with *Eco*RI/*Xho*I restriction sites. The cloned expression vectors for ephrin-$B2_{253-300}$ and ephrin-$B2_{301-333}$ were transformed into the *Escherichia coli* strain BL21 to express GST-fusion proteins which were subsequently purified using glutathione Sepharose (Pharmacia). The cleavage of the fusion proteins was performed by incubating the fusion proteins with bovine factor Xa for 12 h. The purified ephrin-$B2_{253-300}$ peptide was obtained by rebinding the released GST protein to the glutathione Sepharose column while the released ephrin-$B2_{301-333}$ peptide was further purified on an HPLC system using a reverse C_8 column. For heteronuclear NMR experiments, the ephrin-$B2_{253-300}$ and ephrin$B2_{301-333}$ fragments were prepared in ^{15}N-labeled form using a similar expression protocol except for growing *E. coli* cells in the M9 media instead of the 2YT media. The $(^{15}NH_4)_2SO_4$ salt was used for ^{15}N labeling. The identity of the ephrin$B2_{301-333}$ peptide was confirmed by MALDI mass spectrometry.

Peptide Synthesis and Purification. A peptide derived from residues 301−333 of human ephrin B2 was also chemically synthesized using standard FMOC chemistry at the Protein Chemistry Group of the Biotechnology Research Institute. The synthetic peptide was purified by a reverse-phase HPLC C_{18} column eluted with an acetonitrile gradient of 10−50%. The identity of the synthetic peptide was verified by electrospray mass spectrometry and NMR signal assignments.

NMR Sample Preparation. The NMR samples of the recombinant cytoplasmic domain ephrin-$B2_{253-333}$ and the subfragment ephrin-$B2_{253-300}$ were prepared by exchanging the purified samples into 400 μL of 50 mM sodium phosphate buffer (pH 6.8). The concentrations of the ^{15}N-labeled ephrin-$B2_{253-300}$ and ephrin-$B2_{301-333}$ peptides are ~60 μM and 0.9 mM, respectively. Samples of the synthetic 33-residue peptide with peptide concentrations of ~2.5 mM were prepared by dissolving the lyophilized peptides in 400 μL of either H_2O or D_2O aqueous buffer containing 50 mM sodium phosphate. The pH or pD values of the NMR samples were adjusted to 6.8, and deuterated DTT was added to the samples to a final concentration of 15 mM to prevent the formation of intermolecular disulfide. The deuterium lock signal for the NMR spectrometers was provided by the addition of 50 μL of D_2O. The cocktail of protease inhibitors was also added to inhibit the activities of any residual proteases not removed by the purification procedure.

NMR Experiments and Resonance Assignments. NMR experiments were carried out on Bruker Avance-500 or Avance-800 spectrometers equipped with a 5 mm triple-resonance probe with pulse field gradient accessories. Phase-sensitive detection by time-proportional phase incrementation was employed for both the two-dimensional Overhauser effect NOESY (*23*) and the total correlation TOCSY (*24*) experiments. Mixing times of 120 and 200 ms were used for NOESY experiments, and a mixing time of 65 ms for TOCSY experiments. A set of two- and three-dimensional heteronuclear experiments, including HSQC, TOCSY−HSQC, and NOESY−HSQC (ref *25* and references cited therein), were collected for the ^{15}N-labeled protein fragments ephrin-B2$_{253-300}$ and ephrin-B2$_{301-333}$ at 288 K. Spectral processing was carried out using the XwinNMR spectrometer software (Bruker). Sequence-specific assignments of the proton resonances for the synthetic 33-residue peptide ephrin-B2$_{301-333}$ were achieved through identification of spin systems in the TOCSY spectra combined with sequential NOE connectivities in the NOESY spectra (*26*, *27*). The assignment of the ^{15}N-labeled peptide ephrin-B2$_{301-333}$ was achieved by use of HSQC and three-dimensional heteronuclear NMR experiments, HSQC−TOCSY, and HSQC−NOESY. The dihedral angle (ϕ) constraints were converted from $^3J_{\alpha H-NH}$ coupling constants calculated from the separation of cross-peak extrema of a DQF-COSY spectrum acquired at pH 6.8 and 288 K (*28*).

Structure Calculations and Comparison. The structure calculation was based on two NMR data sets at 288 and 298 K. The NOESY spectra for both H_2O and D_2O at two temperatures were peak-picked manually by use of nmrView (*29*). The obtained peak lists were combined with the proton chemical shift assignments using a procedure which excluded all diagonal and probable intraresidue peaks and generated an initial list of ambiguous and unambiguous restraints (*30*). The restraint lists were used as input for ARIA calculations (*31*), together with a list of ϕ dihedral restraints based on a DQF-COSY analysis at 15 °C. An iterative series of ARIA runs using CNS 1.0 (*30*, *32*) was performed, each with the standard 8 iterations. The NOE peaks corresponding to violated restraints were rechecked in the spectra to eliminate noise and artifacts. After the first two runs, NOESY spectra were simulated by an in-house program, PDB2NOE, from the five best structures by assuming the correlation time to be 1500 ps. Based on the difference between the simulated and experimental spectra, the assignments were rechecked and corrected until the simulated spectra strongly resembled the real ones.

Visualization and comparison of structures were carried out by use of the Sybyl molecular graphics program (Tripos Inc.) and the Insight II software package. The coordinates for the three-dimensional structures of the peptide−PDZ and peptide−SH2 complexes were obtained from the Protein DataBank with file names of 1BE9, 1D4W, and 1FU5.

Backbone ^{15}N NMR Relaxation Measurements. ^{15}N $T1$ and $T2$ relaxation times and {^{1}H}-^{15}N steady-state NOEs were determined on the 800 MHz spectrometer at both 278 and 288 K as described previously (*33*, *34*). ^{15}N $T1$ values were measured from HSQC spectra recorded with relaxation delays of 20, 80, 150, 230, 330, 500, 650, 850, 1110, and 1400 ms. ^{15}N $T2$ values were determined with relaxation delays of 14.4, 43.2, 72.0, 115.2, 158.4, 201.6, 244.8, 288.0, 331.2, and 374.4 ms. {^{1}H}-^{15}N steady-state NOEs were obtained by recording spectra with and without ^{1}H presaturation of duration 3 s plus a relaxation delay of 5 s at 800 MHz. The presence of microsecond to millisecond scale conformational exchange processes was assessed by CPMG-based NMR experiments at 288 K, with the repetition rates (or effective $B1$ field strengths) of the CPMG pulse train varying from 100 to 1000 s^{-1} as described previously (*34*−*36*).

RESULTS

NMR Characterization of the Ephrin B2 Cytoplasmic Domain and Ephrin-B2$_{253-300}$, Ephrin-B2$_{301-333}$ Subfragments. The 81-residue cytoplasmic domain of human ephrin B2, expressed and purified as a His-tagged protein, was found to form a gel-like solution and had broad and narrowly dispersed proton NMR signals (not shown), indicating the lack of structure formation and the tendency for aggregation. The formation of the gel-like solution still persisted at pH 5.0 and therefore may not be due to isoelectric precipitation because the pI value of ephrin-B2$_{253-333}$ is predicted to be 9.73. The entire cytoplasmic domain was further dissected into two subfragments: ephrin-B2$_{253-300}$ and ephrin-B2$_{301-333}$. The expressed ephrin-B2$_{253-300}$ fragment aggregated rapidly at neutral pH even at a very low peptide concentration of ~60 μM and even though its pI value is 11.34 in the very basic region. An HSQC spectrum of a freshly prepared ^{15}N-labeled ephrin-B2$_{253-300}$ sample at a concentration of ~30 μM again showed very broad and narrowly dispersed NMR signals, only ~0.8 ppm for the proton and ~17 ppm for the ^{15}N resonances (Figure 2a). Moreover, the peptide sample continued to precipitate even at 4 °C, with only about half of the peptide remaining in solution after 2 weeks. Taken together, these results reveal that the ephrin-B2$_{253-300}$ peptide is also not uniquely structured in solution and is prone to aggregation even at very low concentrations.

In contrast, the expressed ephrin-B2$_{301-333}$ fragment had a well-dispersed ^{1}H-^{15}N HSQC spectrum (Figure 2b) with the HSQC peaks easily assignable to specific residues. The sharp and well-dispersed HSQC cross-peaks indicate the lack of detectable aggregation for the ephrin-B2$_{301-333}$ fragment. Furthermore, a synthetic form of the ephrin-B2$_{301-333}$ fragment showed no detectable changes of its proton NMR spectra at three peptide concentrations: ~2, 1, and 0.5 mM. Also, a MALDI mass spectrum indicated the absence of intermolecular disulfide formation under the experimental conditions (data not shown). Taken together, these results suggest that residues 301−333 of human ephrin B2 may fold into a defined conformation whether in the expressed or synthetic form.

Solution Structure of the Synthetic Ephrin-B2$_{301-333}$ Peptide. Figure 3 shows selected regions of the NOESY spectra containing a large number of medium- and long-range NOEs. In Figure 3a, the NOEs between the αH proton of Asp310 and the NH proton of Gly312, and between the αH proton of Tyr311 and the NH proton of His313 indicate a loop or turn conformation. In Figure 3b, long-range NOEs between His303 and Val318, His303 and Gln319, Lys306 and Tyr316, Glu305 and Tyr316 further reveal the presence of a hairpin structure. The solution conformation of the synthetic ephrin-B2$_{301-333}$ peptide was therefore assessed in further detail

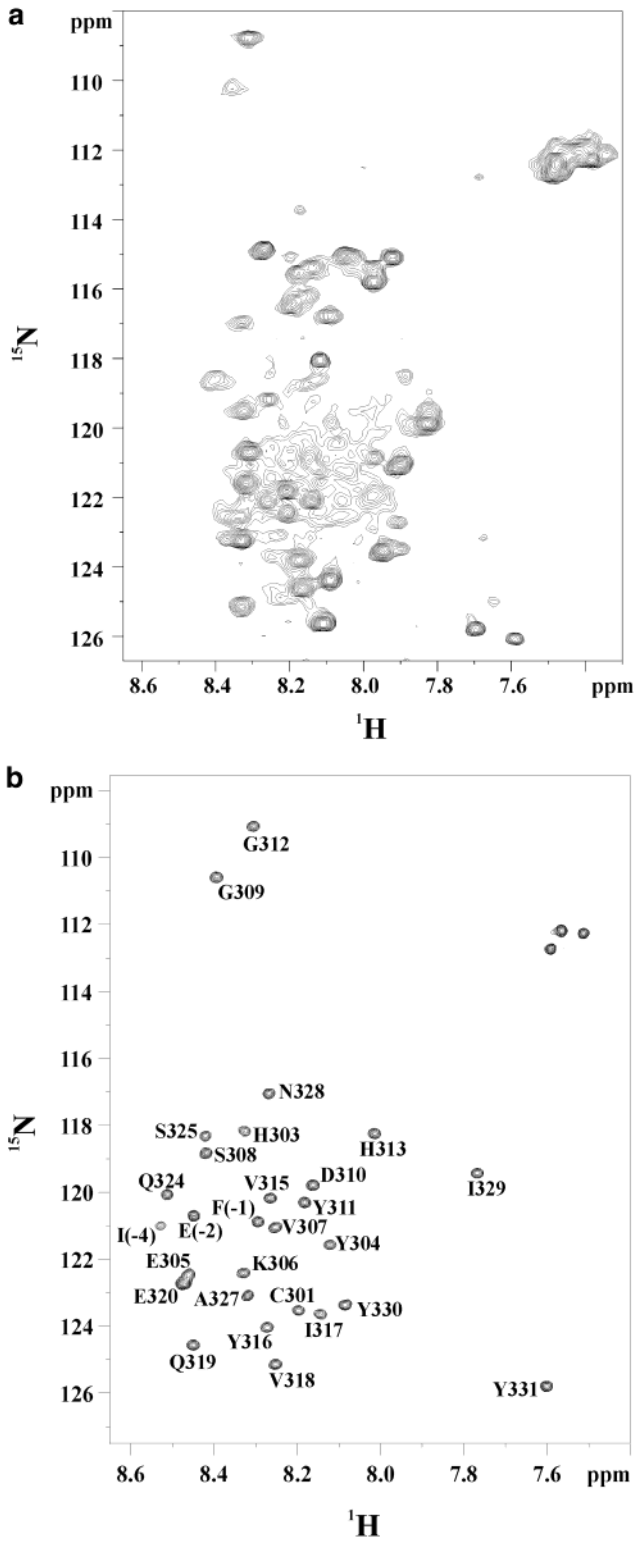

FIGURE 2: ^{1}H-^{15}N HSQC spectra of two subfragments of the cytoplasmic domain of human ephrin B2. (a) HSQC spectrum of the ^{15}N-labeled ephrin-B2$_{253-300}$ in 50 mM phosphate buffer at pH 6.8 and 288 K. (b) HSQC spectrum of the ^{15}N-labeled ephrin-B2$_{301-333}$ in 50 mM phosphate buffer at pH 6.8 and 288 K, with corresponding residues labeled. The additional residues Ile(−4), Glu(−2), and Phe(−1) are from the linker sequence GIPEF attached to the ephrin-B2$_{301-333}$ fragment after the factor Xa cleavage of GST−ephrin-B2$_{301-333}$ fusion protein.

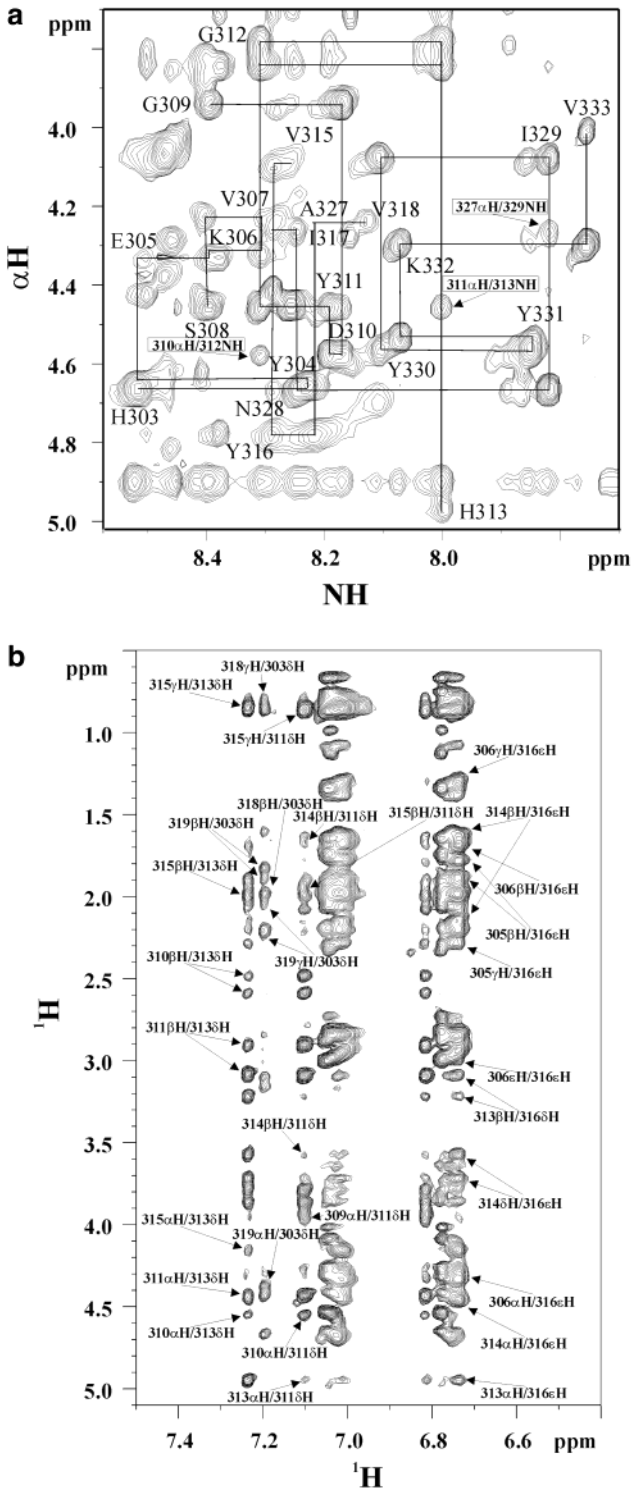

FIGURE 3: Homonuclear NOESY spectra of the synthetic ephrin-B2$_{301-333}$ peptide. (a) NH−αH region of the NOESY spectrum with a mixing time of 200 ms in H_2O at pH 6.8 and 288 K, with sequential assignments and several medium-range NOEs labeled. (b) Aromatic side chain region of a NOESY spectrum with a mixing time of 200 ms in D_2O at pH 6.8 and 288 K. Many key medium- and long-range NOEs are present among specific residues (as labeled), indicating extensive side chain packing interactions.

through structure calculations. A final cluster of 60 structures was generated from 14 dihedral angle constraints and 607 unique and 300 ambiguous constraints. The lowest-energy structures with distance violations less than 0.2 Å and dihedral angle violations less than 5° were selected (a total of eight structures as shown in Figure 4) for the following analysis. The calculation statistics of the eight selected

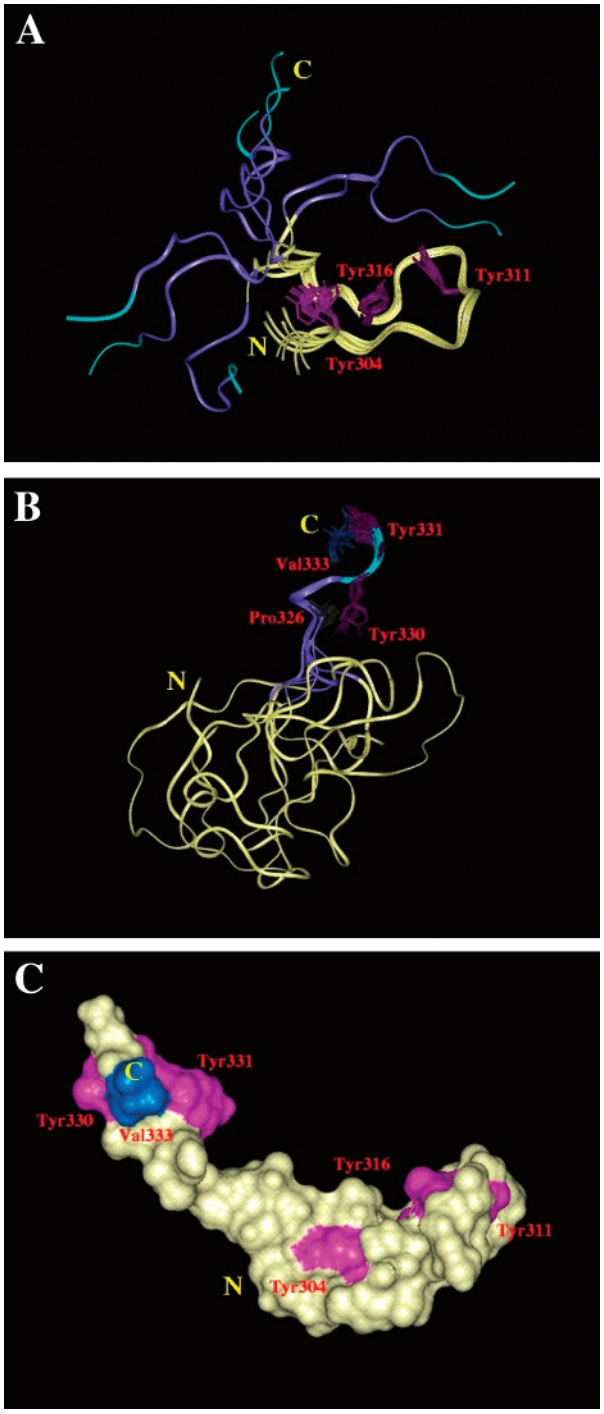

FIGURE 4: Solution structure of the functional subdomain ephrin-B2$_{301-333}$. (a) Ribbon representation of the eight lowest-energy structures superimposed over residues 303−317, with the side chains of Tyr304, Tyr311, and Tyr316 displayed in stick mode and colored in red. Bright yellow is used to color residues 301−322, which is identical to the binding region of ephrin B1 for the SH2 domain of the Grb4 protein when phosphorylated (*21*). Cyan is used to color the PDZ binding motif Tyr330-Tyr331-Lys332-Val333. The rest region is colored in blue. (b) Same eight structures superimposed over residues Pro326−Tyr331. Side chains of Tyr330 and Tyr331 are displayed in stick mode and colored in red. Side chains of Pro326 and Val333 are also displayed in stick mode and colored in gray and blue, respectively. (c) Surface representation of the lowest-energy structure with five functionally important tyrosine residues colored in pink and Val333 in blue.

structures are presented in Table 1. The low values of distance and dihedral restraint energy terms indicate that the

Table 1: Statistics of the Refined Solution Structures of Ephrin-B2$_{301-333}$

structural constraints determined by nmr	
unique distance constraints	
sequential	187
medium- and long-range	420
ambiguous distance constraints	300
Φ dihedral angle constraints	14
energetic parameters	
E(total)	67.2 ± 2.9
E(NOE)	13.1 ± 1.3
E(bond)	2.4 ± 0.2
E(angle)	17.2 ± 1.0
E(improper)	2.2 ± 0.4
E(VdW)	32.1 ± 2.2
rms deviations from idealized geometry	
bond lengths (Å)	0.002 ± 0.000
angles (deg)	0.341 ± 0.010
improper angles (deg)	0.223 ± 0.020

selected eight structures are all consistent with the experimental NMR data. Moreover, the idealized geometry is respected as indicated by the low rms deviations for the bond lengths (0.002 Å) and valence angles (0.34°).

The solution conformation of the ephrin-B2$_{301-333}$ peptide appears to consist of two distinctive structural elements, a well-packed hairpin structure for residues His303−Ile317 followed by a short turn at the C-terminal region over residues Pro326−Lys332. The orientation between these two structural elements seems to be poorly defined, as shown by Figure 4a,b, due to the absence of NOE connectivities between the two segments. The absence of NOE connectivities between the two structural elements most likely results from the flexibility of the ephrin-B2$_{301-333}$ molecule, as indicated by the ^{15}N backbone relaxation data (Figure 5). To further assess the orientation between N- and C-terminal regions, we attempted to extract residual dipolar coupling constants from HSQC spectra of the ^{15}N-labeled ephrin-B2$_{301-333}$ without proton decoupling at both 500 and 800 MHz (*37*). We did not use phages or membrane mimetics to induce alignments since the small and relatively flexible ephrin-B2$_{301-333}$ may interact with membrane surfaces which makes the coupling constants extremely difficult to interpret. The measured residual dipolar coupling constants are all less than 1 Hz, and there is no specific pattern appearing over the sequence (data not shown). This could result from limited alignment and/or averaging of residual dipolar coupling constants by internal motions. Therefore, it appears that the measurements of residual dipolar coupling constants are not suitable for flexible proteins/peptides such as ephrin-B2$_{301-333}$, as pointed out recently (*38*).

The hairpin structure is defined by two strand residues, His303−Val307 and His313−Ile317, linked by a long loop over residues Ser308−Gly312. The average backbone rms deviation among eight structures is only 0.7 Å for the entire hairpin over residues 303−317, and the conformation of the loop Ser308−Gly312 is similar to the omega-loop as described previously (*39*). The hairpin structure appears to lack a classic β-sheet backbone conformation because characteristic αH−NH, αH−αH NOEs between the two strands were not observed. As a consequence, not all Ψ, Φ angles for hairpin residues were located in the β-sheet region of the Ramachandran plot. In contrast, extensive side-chain interactions between two strands were found among the

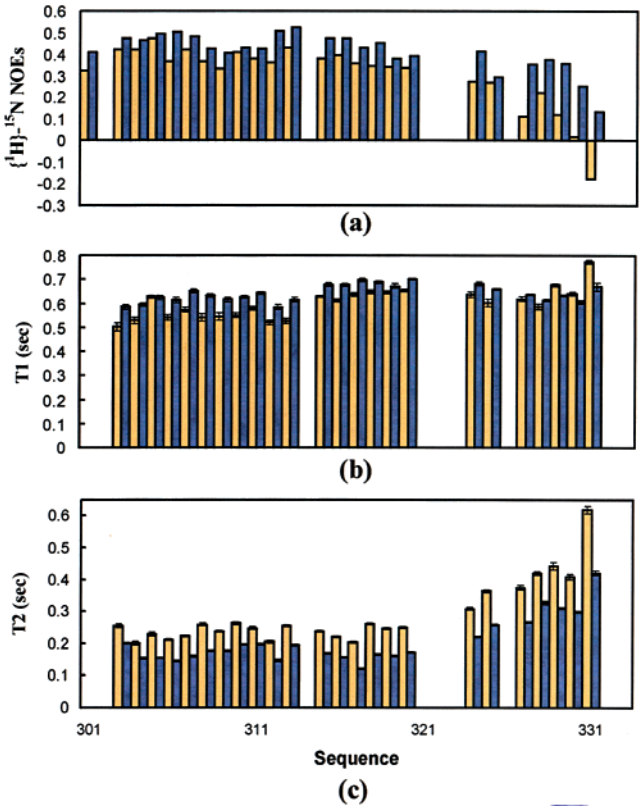

FIGURE 5: Backbone ^{15}N relaxation data of ^{15}N-labeled ephrin-B2$_{301-333}$ at pH 6.8 and different temperatures. (a) {^{1}H}-^{15}N steady-state NOE intensities. (b) ^{15}N *T*1 relaxation times, and (c) ^{15}N *T*2 relaxation times. The yellow bars are used to indicate data at 288 K, and the blue bars are for those at 278 K.

aromatic and hydrophobic residues, such as Pro, His, Tyr, Val, and Ile residues (Figure 3b). Strikingly, this hairpin structure even persisted in a truncated fragment over residues 301−317 (Song et al., unpublished data). This observation suggests that the hairpin structure may be mostly stabilized by a side chain packing network. Interestingly, the strategy to stabilize side chain interaction, in particular those between tyrosine and proline, was successfully used recently to design a 20-residue miniprotein (*40*). It is very surprising that the N-terminal part of the ephrin-B2$_{301-333}$ peptide can form such a well-defined hairpin structure since this hairpin structure is not commonly found for linear peptides in the absence of a disulfide constraint (*41*). The hairpin structure, therefore, is another member of the very small and unusual group of naturally occurring linear peptide sequences which form hairpin conformations.

In contrast, the region over residues Val318−Ser325 is not well-defined, with a backbone rms deviation of 2.4 Å over residues Val318−Ser325. However, as shown in Figure 4b, the C-terminal region over residues Pro326−Lys332 is again well-defined, with an average backbone rms deviation of 0.75 Å among the structures. The secondary structure for Pro326−Tyr330 resembles a distorted turn, which may be stabilized again by the extensive side chain interactions between Pro326 and Tyr330. Moreover, as seen in Figure 4c, out of five functionally important tyrosine residues, the C-terminal two, Tyr330 and Tyr331, are well-exposed while the other three, Tyr304, Tyr311, and Tyr316, are relatively buried in the hairpin fold.

^{15}N Relaxation Measurements and Conformational Dynamics of Ephrin-B2$_{301-333}$. Figure 5 presents the ^{15}N relaxation data of backbone amide nitrogens of the expressed ephrin-B2$_{301-333}$ fragment, including {^{1}H}-^{15}N NOE intensities and *T*1 and *T*2 relaxation times. Most residues have positive heteronuclear NOEs (Figure 5a) with averaged values of 0.28 at 288 K and 0.39 at 278 K, which are quite large for peptides of this size as compared to those reported previously (*34*, *42*, *43*). Generally, the heteronuclear NOEs show a similar pattern at both 278 and 288 K, and NOE intensities at 278 K are slightly larger than those at 288 K. However, it appears that even residues 301−333 can be divided into the N-terminal and C-terminal segments. Residues of the N-terminal part have much larger heteronuclear NOEs than those of the C-terminal part. More precisely, residues His303−Ile317, which adopt a well-packed hairpin structure in the synthetic ephrin-B2$_{301-333}$ peptide (Figure 4), all have heteronuclear NOEs larger than 0.4 at 278 K, with those of Lys306, Gly312, and His313 even larger than 0.5. Also, residues in the N-terminal and C-terminal parts show differential temperature dependence for their heteronuclear NOE intensities. Residues in the C-terminal part show much more profound increases in heteronuclear NOEs at the lower temperature than those in the N-terminal part (Figure 5a), indicating that the N-terminal region of ephrin-B2$_{301-333}$ is much better structured than the C-terminal region (*43*), in complete agreement with structure calculations (Figure 4). This conclusion is further supported by the ^{15}N *T*2 relaxation times (Figure 5c), which again indicate that ephrin-B2$_{301-333}$ is comprised of two distinctive elements. Residues 303−320 have averaged *T*2 values of 0.167 s at 278 K and 0.235 s at 288 K, which are much smaller than those for residues 22−31, with averaged values of 0.262 s at 278 K and 0.367 s at 288 K. Interestingly, no significant response of the ^{15}N *T*2 values to the CPMG pulse delays was observed at 288 K up to the CPMG repetition rate of 1000 s^{-1} for all residues (data not shown), indicating that the conformational exchange for ephrin-B2$_{301-333}$ may either occur on the microsecond time-scale or involve other conformations with small chemical shift deviations, or both (*35*).

DISCUSSION

The present study shows that the entire cytoplamic domain and its N-terminal fragment, ephrin-B2$_{253-300}$, lack the ability to fold into a well-defined three-dimensional structure and are particularly prone to aggregation. Interestingly, clustering of intact ephrin B molecules has been suggested to be critical for its functions (*9*, *22*, *44*−*46*). Moreover, it has been found that Eph receptors can even discriminate specific oligomerization forms to determine alternative signaling pathways (*45*). It has been demonstrated that the extracellular domain of ephrin B2 plays an important role in ligand oligomerization/clustering (9, *22*). We thus speculate that the cytoplasmic domain may also contribute to the oligomerization/clustering of the ephrin B2 molecule relevant to its biological function. Interestingly, the highly conserved 33-residue C-terminal subdomain has no detectable aggregation at concentrations up to 2.5 mM and adopts a well-packed hairpin followed by a mobile tail. It is therefore likely that even the small cytoplasmic domain of ephrin B may consist of two

functional subdomains. The C-terminal 33-residue subdomain may be primarily responsible for interactions with its binding partners such as the PDZ and SH2 domains (*20, 21*), while the N-terminal 48-residue subdomain may mainly participate in ephrin multimerization in response to the binding interactions involving the C-terminal region (*20, 21*).

The central themes for the cytoplasmic half of the bidirectional signaling are interactions between the cytoplasmic domain and its intracellular ligands. The last 33 residues of the cytoplasmic domain, which is the most conserved region among ephrin B molecules, contain all 5 functionally important tyrosine residues and carry all binding sites identified so far (*20, 21*). More specifically, the C-terminal residues of the ephrin-$B2_{301-333}$ fragment, Tyr330-Tyr331-Lys332-Val333, have been identified as the binding motif for a PDZ domain of the PDZ−RGS protein (*20*). The PDZ domains are known to recognize C-terminal sequences in extended conformations (*47, 48*), as exemplified by the peptide structure bound to the third PDZ domain of the PSD-95 protein (*49*). In the solution structure of the ephrin-$B2_{301-333}$ fragment, residues Tyr330-Tyr331-Lys332-Val333 are well-exposed and relatively mobile (Figure 4), making them available for binding interaction. On the other hand, all three ephrin B cytoplasmic tails were found to interact with an SH2 domain of the Grb4 protein in a phosphorylation-dependent manner, and the binding region of ephrin B1 is identical to residues 301−322 of ephrin B2, which form a well-packed hairpin structure (Figure 4a) (*21*). Previously, both phosphorylated and nonphosphorylated peptides bound to SH2 domains have been found to adopt extended conformations (*50*−*53*). Therefore, the well-packed free-state hairpin structure in the ephrin-$B2_{301-333}$ peptide may not be suitable for SH2 binding in the absence of phosphorylation-induced conformational changes (*21*). If one considers that protein tyrosine-phosphorylation usually disrupts or destabilizes the existing secondary structures (*54*−*56*), it is reasonable to assume that conformational changes may also occur upon phosphorylation in a hairpin structure of the ephrin B2 cytoplasmic domain. However, since the in vivo phosphorylation of ephrin B molecules appears to be very complex (*57*), the nature of such conformational changes will still remain obscure until the functionally relevant phosphorylation sites required for SH2 binding can be identified in future studies.

In conclusion, our NMR study provides the first insights into the structural basis for how different functions can be incorporated into the small cytoplasmic domain of human ephrin B2. Even the 33-residue C-terminal functional subdomain can assume two structural elements with distinctive structural and dynamic properties, one serving as a docking site for the PDZ domain of the PDZ−RGS protein and the second for binding to the SH2 domain of the Grb4 protein, connecting to an alternative signaling pathway. The PDZ docking site is located on the exposed and flexible C-terminus, ready for the binding interaction, while the SH2 docking site may be kept cryptic by a well-packed hairpin structure, requiring activation by tyrosine-phosphorylation.

ACKNOWLEDGMENT

We thank Betty Zhu for her help with NOESY back-calculations and Anatol Koutychenko for help with some of the structure calculations.

SUPPORTING INFORMATION AVAILABLE

Proton chemical shifts of ephrin-$B2_{301-333}$ at 288 K and pH 6.8. This material is available free of charge via the Internet at http://pubs.acs.org.

NOTE ADDED AFTER ASAP POSTING

This paper was inadvertently published without the Supporting Information paragraph 08/10/02. The correct version was posted 09/03/02.

REFERENCES

1. Holder, N., and Klein R. (1999) *Development 126*, 2033−2044.
2. Schmucker, D., and Zipursky, S. L. (2001) *Cell 105*, 701−704.
3. Flanagan, J. G., and Vanderhaeghen, P. (1998) *Annu. Rev. Neurosci. 21*, 309−345.
4. O'Leary, D. D., and Wilkinson, D. G. (1999) *Curr. Opin. Neurobiol. 9*, 65−73.
5. Xu, Q., Mellitzer, G., Robinson, V., and Wilkinson, D. G. (1999) *Nature 399*, 267−271.
6. Adams, R. H., and Klein, R. (2000) *Trends Cardiovasc. Med. 10*, 183−188.
7. Patan, S. (2000) *J. Neurooncol. 50*, 1−15.
8. Adams, R. H., Diella, F., Hennig, S., Helmbacher, F., Deutsch, U., and Klein, R. (2001) *Cell 104*, 57−69.
9. Toth, J., Cutforth, T., Gelinas, A. D., Bethoney, K. A., Bard, B., and Harrison, C. J. (2001) *Dev. Cell 1*, 83−92.
10. Kullander, K., Mather, N. K., Diella, F., Dottori, M., Boyd, A. W., and Klein, R. (2001) *Neuron 29*, 73−84.
11. Mellitzer, G., Xu, Q., and Wilkinson, D. G. (1999) *Nature 400*, 77−81.
12. Mellitzer, G., Xu, Q., and Wilkinson, D. G. (2000) *Curr. Opin. Neurobiol. 10*, 400−408.
13. Bennett, B. D., Zeigler, F. C., Gu, Q., Fendly, B., Goddard, A. D., et al. (1995) *Proc. Natl. Acad. Sci. U.S.A. 92*, 1866−1870.
14. Bergemann, A. D., Cheng, H.-J., Brambilla, R., Klein, R., and Flanagan, J. G. (1995) *Mol. Cell. Biol. 15*, 4921−4929.
15. Gale, N. W., Flenniken, A., Compton, D. C., Jenkins, N., Copeland, N. G., Gilbert, D. J., Davis, S., Wilkinson, D. G., and Yancopoulos, G. D. (1996) *Oncogene 13*, 1343−1352.
16. Nicola, N. A., Viney, E., Hilton, D. J., Roberts, B., and Willson, T. (1996) *Growth Factors 13*, 141−149.
17. Tang, X. X., Pleasure, D. E., and Ikegaki, N. (1997) *Genomics 41*, 17−24.
18. Lin, D., Gish, G. D., Songyang, Z., and Pawson, T. (1999) *J. Biol. Chem.* 274, 3726−3733.
19. Bruckner, K., Pablo Labrador, J., Scheiffele, P., Herb, A., Seeburg, P. H., and Klein, R. (1999) *Neuron 22*, 511−524.
20. Lu, Q., Sun, E. E., Klein, R. S., and Flanagan, J. G. (2001) *Cell 105*, 69−79.
21. Cowan, C. A., and Henkemeyer, M. (2001) *Nature 413*, 174−179.
22. Himanen, J. P., Rajashankar, K. R., Lackmann, M., Cowan, C., Henkemeyer, M., and Nikolov, D. B. (2001) *Nature 414*, 933−938.
23. Jeener, J., Meier, B. H., Bachmann, P., and Ernst, R. R. (1979) *J. Chem. Phys. 71*, 4546−4553.
24. Bax, A., and Davis, D. G. (1985) *J. Magn. Reson. 65*, 355−360.
25. Sattler, M., Schleucher, J., and Griesinger, C. (1999) *Prog. NMR Spectrosc. 34*, 93−201.
26. Wagner, G., and Wuthrich, K. (1982) *J. Mol. Biol. 155*, 347−366.
27. Wüthrich, K. (1986) *NMR of Proteins and Nucleic Acids*, John Wiley and Sons, New York.
28. Kim, Y. M., and Prestegard, J. H. (1989) *J. Magn. Reson. 84*, 9−13.
29. Johnson, B. A., and Blevins, R. A. (1994) *J. Biomol. NMR 4*, 603−614.
30. Vranken, W. F., James, S., Bennett, H. P. J., and Ni, F. (2002) *Proteins: Struct., Funct., Genet. 47*, 14−24.
31. Linge, J. P., O'Donoghue, S. I., and Nilges, M. (2001) *Methods Enzymol. 339*, 71−90.
32. Brunger, A. T., Adams, P. D., Clore, G. M., DeLano, W. L., Gros, P., Grosse-Kunstleve, R. W., Jiang, J. S., Kuszewski, J., Nilges, M., Pannu, N. S., Read, R. J., Rice, L. M., Simonson, T., and

Warren, G. L. (1998) *Acta Crystallogr., Sect. D: Biol. Crystallogr. 54* (Pt. 5), 905−921.
33. Farrow, N. A., Muhandiram, R., Singer, A. U., Pascal, S. M., Kay, C. M., Gish, G., Shoelson, S. E., Pawson, T., Forman-Kay, J. D., and Kay, L. E. (1994) *Biochemistry 33*, 5984−6003.
34. Song, J., Chen, Z., Xu, P., Gingras, R., Ng, A., Leberer, E., Thomas, D. Y., and Ni, F. (2001) *J. Biol. Chem. 44*, 41205−41212.
35. Millet, J. O., Loria, P., Kroenke, C. D., Pons, M., and Palmer, A. G., III (2000) *J. Am. Chem. Soc. 112*, 2867−2877.
36. Mulder, F. A. A., Skrynnikov, N. R., Hon, B., Dahlquist, F. W., and Kay, L. E. (2001) *J. Am. Chem. Soc. 123*, 967−975.
37. Tolman, J. R., Flanagan, J. M., Kennedy, M. A., and Prestegard, J. H. (1995) *Proc. Natl. Acad. Sci. U.S.A. 92*, 9279−9283.
38. Tolman, J. R., Al-Hashimi, H. M., Kay, L. E., and Prestegard, J. H. (2001) *J. Am. Chem. Soc. 123*, 1416−1424.
39. Fetrow, J. S. (1995) *FASEB J. 9*, 708−717.
40. Neidigh, J. W., Fesinmeyer, R. M., and Andersen, N. H. (2002) *Nat. Struct. Biol. 9*, 425−430.
41. Blanco, F., Ramirez-Alvarado, M., and Serrano, L. (1998) *Curr. Opin. Struct. Biol. 8*, 107−111.
42. Bai, Y., Chung, J., Dyson, H. J., and Wright, P. E. (2001) *Protein Sci. 10*, 1056−1066.
43. Campbell, A. P., Spyracopoulos, L., Irvin, R. T., and Sykes, B. D. (2000) *J. Biomol. NMR 17*, 239−255.
44. Davis, S., Gale, N. W., Aldrich, T. H., Maisonpierre, P. C., Lhotak, V., Pawson, T., Goldfarb, M., and Yancopoulos, G. D. (1994) *Science 266*, 816−819.
45. Stein, E., Lane, A. A., Cerretti, D. P., Schoecklmann, H. O., Schroff, A. D., Van Etten, R. L., and Daniel, T. O. (1998) *Genes Dev. 12*, 667−678.
46. Himanen, J. P., Henkemeyer, M., and Nikolov, D. B. (1998) *Nature 396*, 486−491.
47. Harrison, S. C. (1996) *Cell 86*, 341−343.
48. Songyang, Z., Fanning, A. S., Fu, C., Xu, J., Marfatia, S. M., Chishti, A. H., Crompton, A., Chan, A. C., Anderson, J. M., and Cantley, L. C. (1997) *Science 275*, 73−77.
49. Doyle, D. A., Lee, A., Lewis, J., Kim, E., Sheng, M., and MacKinnon, R. (1996) *Cell 85*, 1067−1076.
50. Koch, C. A., Anderson, D., Moran, M. F., Ellis, C., and Pawson, T. (1991) *Science 252*, 668−674.
51. Kuriyan, J., and Cowburn, D. (1997) *Annu. Rev. Biophys. Biomol. Struct. 26*, 259−288.
52. Poy, F., Yaffe, M. B., Sayos, J., Saxena, K., Morra, M., Sumegi, J., Cantley, L. C., Terhorst, C., and Eck, M. J. (1999) *Mol. Cell 4*, 555−561.
53. Weber, T., Schaffhausen, B., Liu, Y., and Gunther, U. L. (2000) *Biochemistry 39*, 15860−15869.
54. Mortishire-Smith, R. J., Pitzenberger, S. M., Burke, C. J., Middaugh, C. R., Garsky, V. M., and Johnson, R. G. (1995) *Biochemistry 34*, 7603−7613.
55. Szilak, L., Moitra, J., Krylov, D., and Vinson, C. (1997) *Nat. Struct. Biol. 4*, 112−114.
56. Steinmetz, M. O., Jahnke, W., Towbin, H., Garcia-Echeverria, C., Voshol, H., Muller, D., and van Oostrum, J. (2001) *EMBO Rep. 2*, 505−510.
57. Kalo, M. S., Yu, H. H., and Pasquale, E. B. (2001) *J. Biol. Chem. 276*, 38940−38948.

BI025815U